Spatial control of localized oscillations in arrays of coupled laser dimers

Jonial Shena ⬤[*]

National University of Science and Technology MISiS, 4 Leninsky Avenue, Moscow 119049, Russia

Yannis Kominis

School of Applied Mathematical and Physical Science, National Technical University of Athens, 157 80 Athens, Greece

Anastasios Bountis

Department of Mathematics, School of Science and Technology, Nazarbayev University, Astana, Republic of Kazakhstan

Vassilios Kovanis

Bradley Department of Electrical and Computer Engineering, Northern Virginia, Virginia Polytechnic Institute and University, Blacksburg, Virginia 24060, USA

Arrays of coupled semiconductor lasers are systems possessing radically complex dynamics that makes them useful for numerous applications in beam forming and beam shaping. In this work, we investigate the spatial controllability of oscillation amplitudes in an array of coupled photonic dimers, each consisting of two semiconductor lasers driven by differential pumping rates. We consider parameter values for which each dimer's stable phase-locked state has become unstable through a Hopf bifurcation and we show that, by assigning appropriate pumping rate values to each dimer, high-amplitude oscillations coexist with negligibly low-amplitude oscillations. The spatial profile of the amplitude of oscillations across the array can be dynamically controlled by appropriate pumping rate values in each dimer. This feature is shown to be quite robust, even for random detuning between the lasers, and suggests a mechanism for dynamically reconfigurable production of a large diversity of spatial profiles of laser amplitude oscillations.

I. INTRODUCTION

Laser arrays constitute a large family of nonlinear coupled systems which can exhibit a wide variety of complex dynamical behaviors. Although the emission from an individual laser is often stable, the coupled system can display synchronization, spatiotemporal collective phenomena [1–3], and chaotic responses [4–7]. In recent years, there have been many studies concerning semiconductor lasers and their synchronization properties including the occurrence of chimera states [8–11]. This rich set of dynamical features supported by coupled-laser arrays is a result of the interplay between three key characteristics related to nonlinearity due to the coupling between photon and carrier population dynamics [12], non-Hermiticity due to the presence of gain and loss [13,14], and inhomogeneity due to the differential pumping and varying properties of individual lasers.

Moreover, these dynamical features allow for many technological applications in photonic integrated devices that can be dynamically controlled in order to provide a reconfigurable and multifunctional response [15]. In this direction, the consideration of differentially pumped coupled lasers has revealed a new set of interesting dynamical features enabling the

control of the output spectrum of the system in terms of the existence of exceptional points and spectral transitions [16,17], tunable oscillations [18], and tailored modulation responses [19], as well as the spatial distribution of the electric field amplitude in terms of the existence of stable asymmetric phase-locked states [20] and localized synchronization [18,21]. The latter enables important technological applications related to beam forming and steering [22,23]. In these studies, the role of the current injection provides an efficient mechanism for control of the phase-locked and the oscillatory states of the system under a rich set of alternative options in the parameter values of the system that facilitate practical applications. The inhomogeneous pumping as well as the frequency detuning between coupled lasers introduces a system asymmetry and results in carrier densities above and below threshold, with gain and loss coefficients of opposite signs in each laser, so that the respective electric fields experience varying gain and loss resulting in a large variety of spatial profiles for the electric field accross the coupled-laser array. It is noteworthy that the existence of a large variety of spatially localized wave profiles in photonic structures with inhomogeneous gain and loss distributions has also been shown in other discrete [24] and continuous [25] photonic systems; however, in these cases the gain and loss distributions were fixed and could not be controlled dynamically as in the case of inhomogeneously pumped laser arrays.

---

[*]jonialdshena@misis.ru

In the present work, we investigate the collective behavior of a large array of evanescently coupled semiconductor dimers with nearest-neighbor interactions and focus on the possibilities of controlling the spatial profile of amplitude oscillations by applying appropriate pumping distribution patterns. In order to understand the underlying mechanism allowing for large differences in the oscillation amplitude between different lasers in the same array, we start our investigation with a simple dimer and show that the two lasers can demonstrate remarkably large differences in oscillation amplitude. Proceeding to a linear array of two coupled dimers we show that an appropriate pumping pattern can be applied in order to have large oscillations in only one laser while the electric fields of the other three remain almost constant. Based on these results we investigate the possibility of controlling the oscillation amplitude of specific groups of lasers in a large circular array by applying appropriate pumping schemes, characterized by different values in different groups of lasers. We show that, similarly to the smaller arrays, we have coexistence of high-amplitude oscillations for selected groups compared with negligibly low-amplitude oscillations for other groups. These groups of lasers can be either distributed along the array or localized, as we show for the extreme case where the pumping scheme is chosen in order to result in high-amplitude oscillations of only one laser in the array. The characteristic cases suggest that by choosing an appropriate pumping scheme it is possible to control (a) the part of the array where large oscillations take place and (b) the distribution of the oscillation amplitudes within this part. Among the crucial parameters for the control of the dynamical features, namely, the coupling, the optical frequency detuning between the lasers, and the pumping rates, only the latter is dynamically controllable and can be used to control the spatial profile of the oscillation amplitudes of the electric fields

across the array. This results in a remarkable reconfigurability of the system since different spatial patterns of oscillations can be dynamically generated in the same array, suggesting a mechanism with potential applications in multifunctional photonic devices.

II. THE MODEL

The dynamics of an array of coupled laser dimers is governed by the following rate equations for the slowly varying complex amplitude E_j of the electric field of each laser and the corresponding population inversion N_j [10,13,20],

$$\frac{dE_j}{dt} = (1 - ia)N_j E_j + i\eta(E_{j+1} + E_{j-1}) + i\omega_j E_j, \quad (1a)$$

$$T\frac{dN_j}{dt} = P_j - N_j - (1 + 2N_j)|E_j|^2, \quad (1b)$$

where $1 \leqslant j \leqslant M$, M being the number of lasers. The dimensionless time t and the population inversion decay time T are measured in units of the photon lifetime τ_p. a is the line-width enhancement factor resulting in the amplitude – phase coupling. P_j are the normalized pumping rates. η is the normalized coupling rate between neighboring lasers due to interaction through their evanescent fields [26], and the normalized angular frequency ω_j measures the detuning of each laser from a common reference value.

Before proceeding to the investigation of the dynamics of a large array of coupled lasers, we consider the case of a single dimer to gain a better understanding of its dynamics. For equal pumping rates and in the absence of detuning, there exist two phase-locked states with 0 and π phase differences between the two electric fields, which are stable for $\eta > aP/(1 + 2P)$ and $\eta < (1 + 2P)/2aT$, respectively [27].
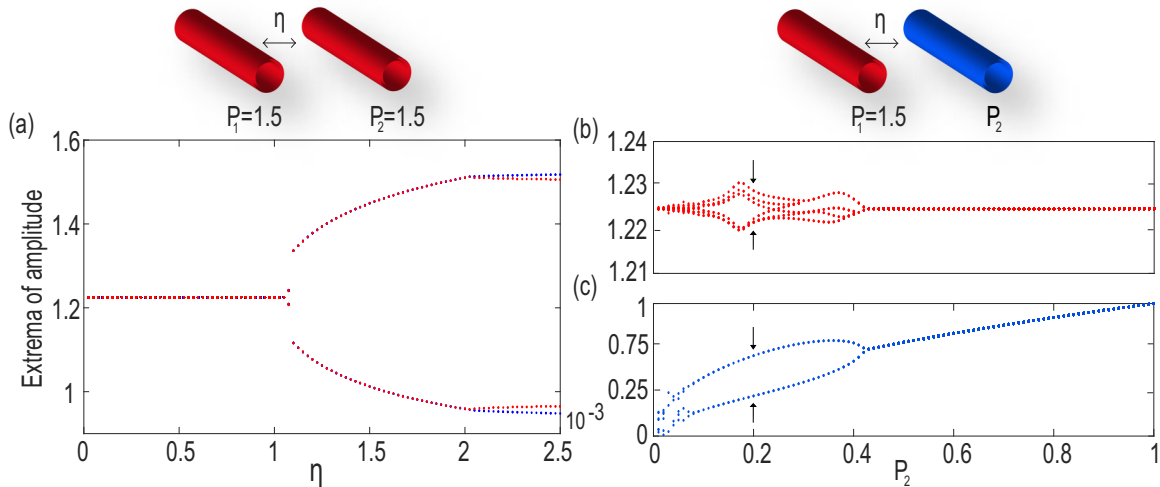

FIG. 1. Bifurcation diagrams for a single laser dimer. (a) Dependence of the extrema of the electric field amplitudes on the coupling strength for two identical lasers with $P_1 = P_2 = 1.5$. Red color refers to the first laser, and blue to the second laser. The steady state is shown to undergo a Hopf bifurcation at $\eta = 0.001pl$, 13. Beyond the Hopf point, for values of η greater than 0.002, we observe different amplitude extrema for each laser. (b), (c) Extrema of the amplitudes of the electric fields as the second laser's pumping rate is varied, at a constant coupling strength $\eta = 0.0005$ and $P_1 = 1.5$. First laser (b) and second laser (c). The steady state undergoes a reverse Hopf bifurcation at $P_2 = 0.42$. The asymmetry of the pumping rates drives the system to a stable limit cycle, with very low amplitudes of oscillation in (b) coexisting with much higher oscillation amplitudes shown in (c). Other parameters are $a = 5$, $T = 400$, and $\omega_j = 0$.
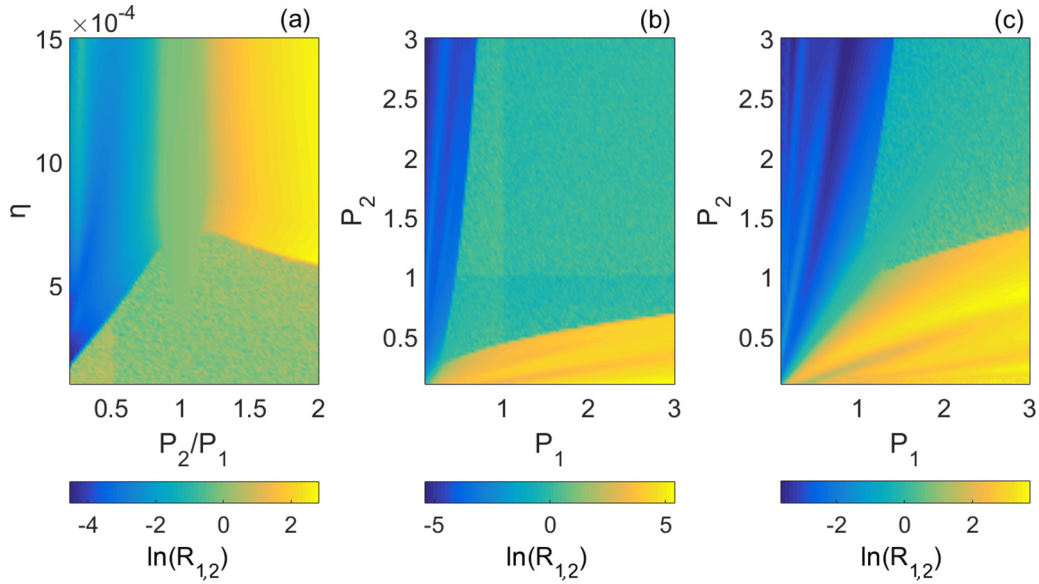
FIG. 2. Ratio of the peak-to-peak oscillation amplitudes $R_{1,2} = E_{1(\text{p-p})}/E_{2(\text{p-p})}$ for the single dimer as a function of the pumping rates $P_{1,2}$ and the coupling strength η. (a) Varying η and pumping rate ratio P_2/P_1 for $P_1 = 0.5$. (b), (c) Varying pumping rates $P_{1,2}$ for $\eta = 0.0005$ and $\eta = 0.0012$, respectively. The ratio deviates significantly from unity when the pumping rates are sufficiently far from $P_1 = P_2$, with the coupling strength determining the appropriate distance from the line $P_1 = P_2$ for a significant asymmetry of oscillation amplitudes. All other parameters are as in Fig. 1.

To understand the effect of the coupling strength, we plot in Fig. 1(a) a bifurcation diagram of the maxima and minima of the amplitudes of the electric fields when the lasers have equal pumping rates set to $P = 1.5$. Varying the coupling parameter, we see that a Hopf bifurcation to a stable limit cycle occurs at $\eta = 0.001\,13$. As the coupling is further increased, to values of η greater than 0.002, the limit cycle of the system is characterized by oscillations with different amplitude extrema for each individual laser. This leads to a slightly asymmetric limit cycle bifurcating from a symmetric one, even under symmetric pumping [18].

Next, keeping the coupling strength at the steady-state value $\eta = 0.0005$, we calculate in Figs. 1(b) and 1(c) a bifurcation diagram, varying P_2 and keeping $P_1 = 1.5$ fixed. The steady state is now seen to undergo a reverse Hopf bifurcation at $P_2 = 0.42$. Below this value, the first laser demonstrates multiple harmonics with amplitudes of different magnitudes corresponding to the same limit cycle [28]. Remarkably, the
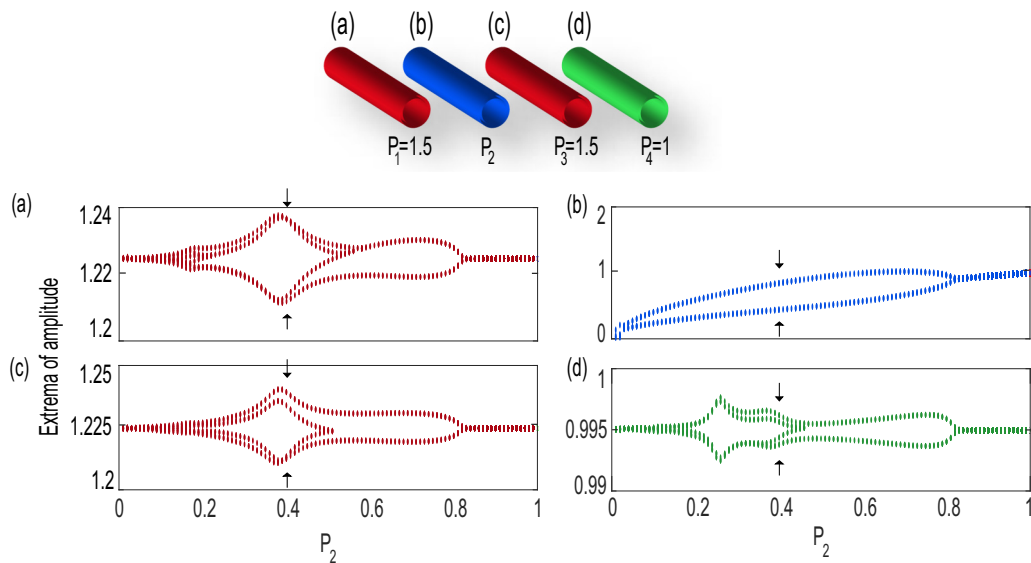

FIG. 3. Bifurcation diagrams for two coupled dimers. Dependence of extrema of the electric field amplitudes on the second laser's pumping rate for each laser, under inhomogeneous pumping. (a) First laser; (b) second laser; (c) third laser; (d) fourth laser. The phase-locked state undergoes a Hopf bifurcation at $P_2 = 0.82$. All field amplitudes of the system are oscillating close to a fixed point, except for the second laser, which exhibits much larger amplitude extrema. The pumping rates are $P_1 = P_3 = 1.5$ and $P_4 = 1$. All other parameters are as in Fig. 1.
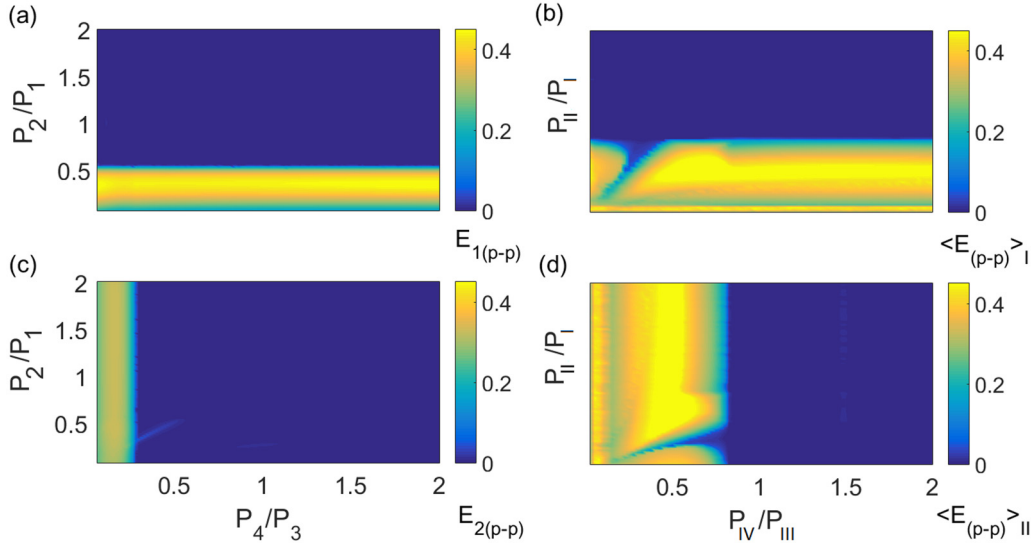
FIG. 4. (a) Peak-to-peak oscillation amplitude for the second and fourth lasers of a coupled dimer as a function of the pumping rate ratios P_2/P_1 and P_4/P_3 for $P_1 = P_3 = 1.5$ and $\eta = 0.0005$. The peak-to-peak oscillation amplitudes for the first and the third lasers (not shown here) are very low. (b) Peak-to-peak oscillation amplitude for the second and fourth groups of lasers of the circular array as a function of the pumping rate ratios P_{II}/P_I and P_{IV}/P_{III} for $P_I = P_{III} = 1.5$ and $\eta = 0.0005$. The peak-to-peak oscillation amplitudes for the first and the third groups (not shown here) are very low. All other parameters are as in Fig. 3 and Fig. 5. Remarkably the same dependence of the dynamical behavior on the pumping rates holds for either four different lasers or four different groups of lasers.

oscillation amplitude of the first laser is much lower than that of the second one, as shown in Figs. 1(b) and 1(c), respectively. Both lasers oscillate around mean values that correspond to a previously stable asymmetric phase-locked state. However, although the oscillations of the second laser have small mean values, they possess considerably higher peak-to-peak amplitude values in comparison to the first one. As shown in Figs. 1(b) and 1(c), in the case where $P_2 = 0.2$ (marked by arrows), the peak-to-peak oscillation amplitude for the second laser is $E_{2(p\text{-}p)} = 0.4214$, whereas the first laser has a peak-to-peak oscillation amplitude $E_{1(p\text{-}p)} = 0.0072$, resulting in a ratio $R_{1,2} = E_{1(p\text{-}p)}/E_{2(p\text{-}p)} = 0.0170$. This behavior is absent for equal pumping and is crucial for the study of a large array of coupled dimers carried out in the next section. The asymmetry characteristics as well as the frequencies of such limit cycles at the Hopf points have recently been studied by Kominis *et al.* [18]. Moreover, as shown in Fig. 2 this behavior is typical in the parameter space of the dimer; for sufficiently different pumping rates, the ratio of the peak-to-peak oscillation amplitudes of the two lasers can be made significantly different from unity (up to many orders of magnitude) with the appropriate pumping difference as well as the maximum ratio values, depending on the coupling strength.

Following the same steps as in the above analysis, it is instructive to plot in Fig. 3 similar bifurcation diagrams for a system of two coupled dimers with different pumping rates ($P_1 = P_3 = 1.5$ and $P_4 = 1$), keeping the coupling strength at the value $\eta = 0.0005$ and varying P_2 as a control parameter. For low values of P_2, a limit cycle exists with multiple harmonics, until $P_2 = 0.82$, where the Hopf bifurcation occurs. Beyond that value, the system regains stability of the steady state and remains stable as P_2 continues to increase up to $P_2 = 1$. Thus, through this choice of pumping param-

eters, it is shown that, in analogy to the previous case of a single dimer, the system as a whole supports an asymmetric localized oscillation where the second laser undergoes high oscillation amplitudes, whereas the other three oscillate with much lower amplitudes for a large range of P_2 values. More specifically, in the case where $P_2 = 0.4$, the peak-to-peak oscillation amplitude of the second laser is $E_{2(p\text{-}p)} = 0.4851$, where the ratio of the peak-to-peak oscillation amplitudes of the other lasers to that of the second laser are $R_{1,2} = 0.053$, $R_{3,2} = 0.064$, and $R_{4,2} = 0.0049$. The dependence of the peak-to-peak oscillation amplitude on the pumping rate ratios is depicted in Fig. 4, where it is shown that the lasers with lower pumping rates have significantly higher oscillation amplitudes. A generalization of this effect to the case of a large array of coupled dimers is studied in the next section.

III. AN ARRAY OF COUPLED-LASER DIMERS

Let as now turn to a large circular array of coupled diode lasers, with nearest-neighbor coupling and an inhomogeneous pumping distribution, as shown in Fig. 5(a). The network is divided into two clusters with two interfaces or into four groups where the elements in the first group are pumped at rates $P_j^I = 1.5$ for $j \in [1, 3, 5, \ldots, M/2 - 1]$, the elements in the second group at $P^{II} = 0.4$ for $j \in [2, 4, 6, \ldots, M/2]$, and those in the third group at $P^{III} = 1.5$ for $j \in [M/2 + 1, M/2 + 3, \ldots, M - 1]$, while in the fourth we set $P_j^{IV} = 1.0$ for $j \in [M/2 + 2, M/2 + 4, \ldots, M]$. To reveal its dynamics we integrate Eqs. (1) using a fourth-order Runge-Kutta algorithm and employ initial conditions with random phases taken from a uniform distribution over the interval $[-\pi$ to $\pi]$, as well as random amplitudes and inverse populations. In all the numerical calculations performed in arrays consisting of 200
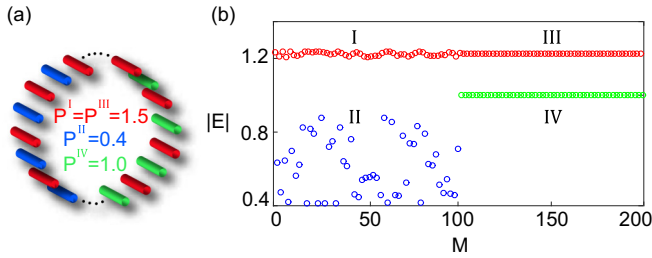
FIG. 5. (a) Schematic of a circular array of 200 coupled lasers with inhomogeneous pumping. The array has been divided into two parts consisting of differently pumped dimers (four groups), where the dimers on the left are pumped with $P^{\mathrm{I}} = 1.5$ (red symbols; first group) and $P^{\mathrm{II}} = 0.4$ (blue symbols; second group) while the dimers on the right have $P^{\mathrm{III}} = 1.5$ (red symbols; third group) and $P^{\mathrm{IV}} = 1$ (green symbols; fourth group). (b) Snapshots of the amplitude of the electric fields in an array of $M = 200$ lasers with inhomogeneous pumping as in the model shown in (a). Only group II is shown to oscillate with high amplitudes, while all others undergo small oscillations close to the fixed point. All other parameters are as in Fig. 1.

lasers, we have not observed any dependence on the initial conditions.

In Fig. 5(b), we plot snapshots of the amplitude of the electric field for an array of $M = 200$ lasers with inhomogeneous pumping distributed as in Fig. 5(a), after a sufficiently long time, $t = 2 \times 10^5$, to show the system's response after transient effects. The coupling strength between the neighbors is equal to $\eta = 0.0005$. The present system represents an extension of the four-laser model depicted in Fig. 3 for the specific value of $P_2 = 0.4$ (marked by arrows). Under the applied distribution of pumping rates, the lasers in group II (blue) support high amplitudes, whereas the remaining groups demonstrate low amplitudes very close to the steady state. Remarkably, the dependence of the oscillation amplitudes of the four groups on the pumping rates is similar to the case of
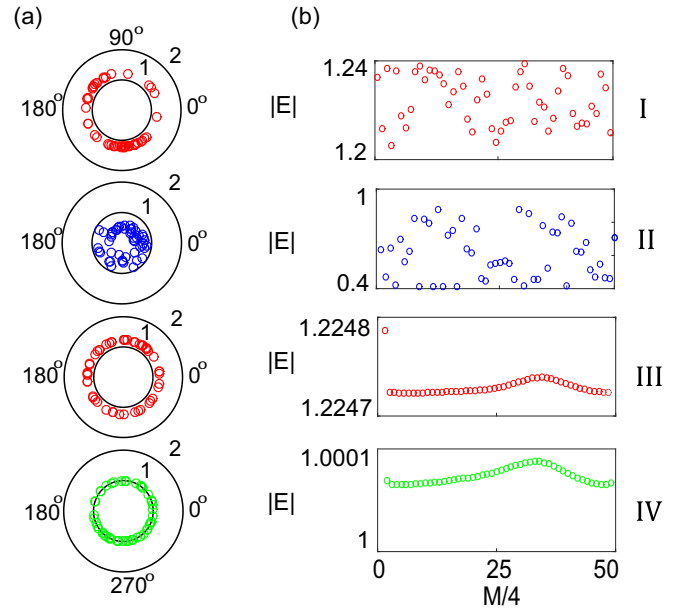

FIG. 6. Snapshots of (a) the complex electric field distributions in the complex plane and (b) the electric field amplitude for all four groups as in Fig. 5.

two coupled dimers, as shown in Fig. 4. This pumping scheme is indicative of the possibility of controlling not only the part of the array where high-amplitude oscillations take place (half of the circular array) but also the spatial pattern of amplitude oscillations within this part (binary pattern of alternating high and negligible amplitudes).

Snapshots of complex electric field distributions for every particular group are shown in Fig. 6(a). The behavior is similar to that of the four coupled lasers, where the second cluster attains high field amplitudes, while the other three oscillate close to the steady state. In Fig. 6(b) we display the
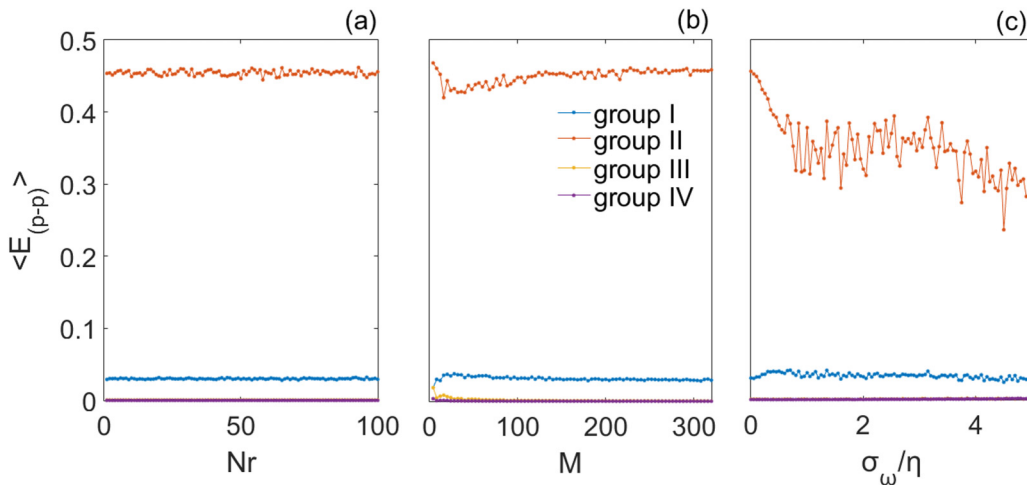

FIG. 7. (a) Average peak-to-peak oscillation amplitudes for each group of lasers for different sets of initial conditions (labeled by an increasing number Nr), for the circular array system with parameters as in Fig. 5. (b) Dependence of the average peak-to-peak oscillation amplitudes for each group of lasers on the system size M (all other parameters as in Fig. 5). (c) Dependence of the average peak-to-peak oscillation amplitudes for each group of lasers on the randomness of laser detunings. The detunings ω_j for all four groups are chosen from a normal random distribution with mean 0 and standard deviation σ_ω normalized to the coupling strength (all other parameters as in Fig. 5).
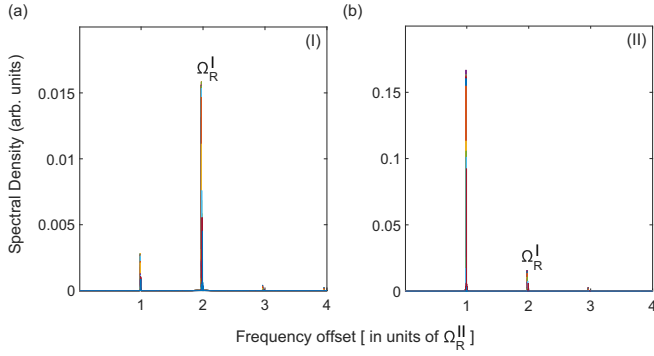
FIG. 8. Fourier power spectra for all the lasers in groups I and II shown in Fig. 5(b). The characteristic frequencies Ω_R^I and Ω_R^{II} are the normalized free-running laser relaxation oscillation frequencies of each individual laser in groups I and II, respectively, with $\Omega_R^I \simeq 2\Omega_R^{II}$.

magnitudes and phases of these states depicted in the complex plane. Evidently, groups I, III, and IV exhibit low-amplitude oscillations, whereas group II undergoes high-amplitude oscillations. Groups III and IV have a smooth amplitude distribution, in sharp contrast to groups I and II. All groups have randomly distributed phases.

The dependence of the peak-to-peak oscillation amplitudes of the different groups of lasers on the initial conditions is depicted in Fig. 7(a) for a circular array with parameters as in Fig. 5; it is clearly shown that the same behavior of localized oscillations holds for a large number of different sets of initial conditions. Moreover, as shown in Fig. 7(b) this behavior is typical for different system sizes (M). Finally, the coexistence of high and low oscillation amplitudes in the different groups of lasers is shown to be robust under quite large randomness of the detunings of each laser, as shown in Fig. 7(c). The above properties facilitate the experimental observation and the exploitation of this dynamical behavior for technological applications.

Regarding the spectral content of the oscillations in each group, shown in Fig. 8, both group I and group II have

the same fundamental frequency, which is close to the free-running relaxation frequency of group II, given as $\Omega_R^{II} = \sqrt{\frac{2P_2}{T}}$, and also have a second spectral peak close to $2\Omega_R^{II}$, which is also very close to $\Omega_R^I = 1.94\Omega_R^{II}$ for the specific choice of pumping parameters. However, the relative power of the two spectral components is reversed in the two groups of lasers.

In order to investigate the phase coherence of each group in time, we calculate the radius of the complex order parameter [29]

$$r(t) = \frac{1}{N}\left|\sum_{j=1}^{N} e^{i\phi_j}\right|, \qquad (2)$$

where N is the number of lasers in each group and ϕ_j the phase of the jth laser. If the group is coherent in phase, we have $r(t) \simeq 1$. On the other hand, if the group is incoherent, then $r(t) \simeq 0$. In Figs. 9(a)–9(d) we present the order parameter for groups I, II, III, and IV oscillating as in Fig. 5, respectively. The oscillations of the order parameter for all the groups under 0.5 indicate the lack of phase synchronization between the lasers in each group as also shown in the snapshot in Fig. 6.

To estimate the spatial coherence of the electric field amplitudes under time evolution, we use, as an appropriate quantity, the local curvature of the electric field amplitude distribution within each laser group calculated for the sufficiently long time interval of 2×10^5 [30]. This is done by applying the discrete Laplacian DE on the spatial data of the amplitude of the electric field as follows:

$$\text{DE}_j(t) = |E_{j+1}(t)| + |E_{j-1}(t)| - 2|E_j(t)|. \qquad (3)$$

Figure 10 shows the spatiotemporal evolution of the absolute values of the local curvature on a logarithmic scale corresponding to the oscillations shown in Fig. 5(b). The local curvature, properly rescaled with respect to its maximum and minimum values, is shown to be significantly larger for group II in comparison to the other laser groups. This particular behavior holds for any system size and suggests the possibility
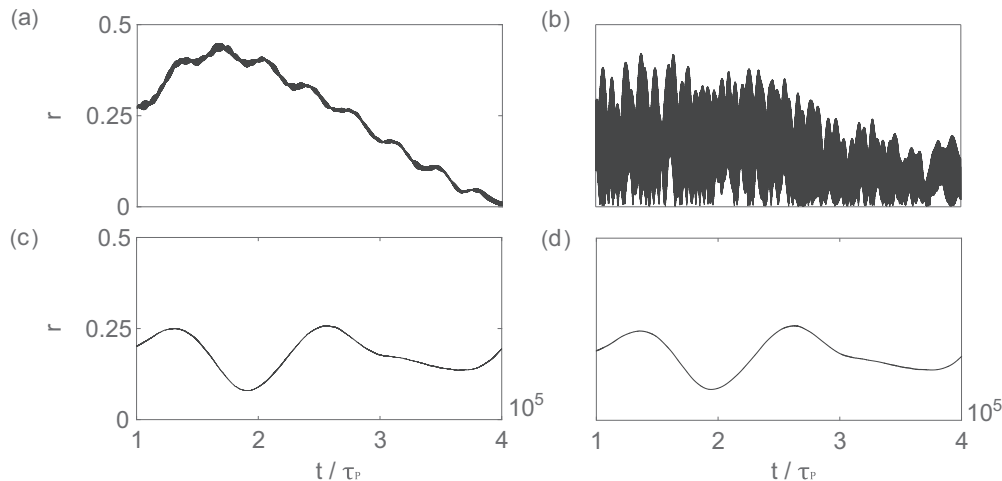

FIG. 9. (a)–(d) Radius of the complex order parameter for laser oscillations in groups I, II, III, and IV for a system as in Fig. 5, on average over time, indicating the lack of phase synchronization.
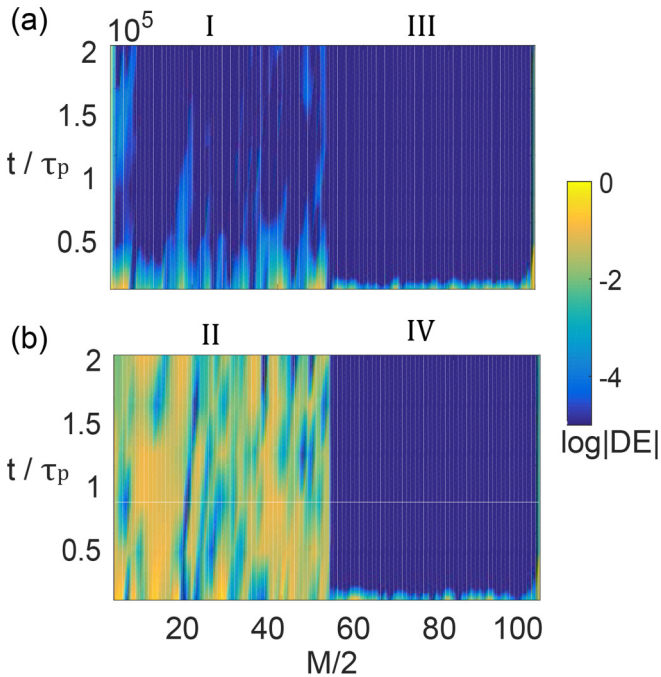
FIG. 10. Temporal evolution of the local curvature $|DE(t)|$ on a logarithmic scale, for the array in Fig. 5. For low oscillation amplitudes close to the steady state, as in groups I, III, and IV, the local curvature, properly rescaled with its maximum and minimum, is lower than 10^{-4}, indicating very uniform amplitude distributions, in contrast with the high amplitudes in case II, where the local curvature takes values close to unity. All other parameters are as in Fig. 5.

FIG. 11. Temporal evolution of the local curvature $|DE(t)|$ on a logarithmic scale as in Fig. 10, in the presence of detuning. The detunings ω_j for all four groups are chosen from a normal random distribution with mean 0 and standard deviation $\sigma_\omega = 3\eta$. The behavior of the system is similar to that shown in Fig. 10, implying that the coexistence of small and large oscillations remains robust even for large values of detuning. All other parameters are as in Fig. 5.

of achieving control of spatial patterns of large and small oscillations.

In all previous calculations, it has been assumed that the frequency detuning between all lasers is equal to 0. However, we have carried out an extensive study of what happens in the presence of detuning as follows: In Fig. 11, the temporal evolution of the local curvature is presented for the electric field amplitudes shown in Fig. 5(b), where the detunings ω_j have been chosen from a normal random distribution with mean 0 and standard deviation equal to $\sigma_\omega = 3\eta$. Note that a proper consideration of the level of detuning must be made in relation to the coupling strength [31,32]. In comparison to Fig. 10, it is evident that all the qualitative characteristics of oscillation amplitude behaviors are quite robust even under the presence of strong random detuning.

As an example of extremely localized oscillations, we consider the case where only one laser in the array exhibits high-amplitude oscillations, while all other lasers in the system are close to a steady state. Such a configuration is schematically presented in Fig. 12(a), where all lasers are assigned pumping rate values alternating between $P = 1.5$ and $P = 1.0$ except the central laser, which has $P = 0.4$. Under this pumping distribution, Fig. 12(b) displays a snapshot of the electric fields for the whole system, where the middle laser undergoes "breatherlike" localized oscillations [33,34]. The temporal evolution of the local curvature corresponding
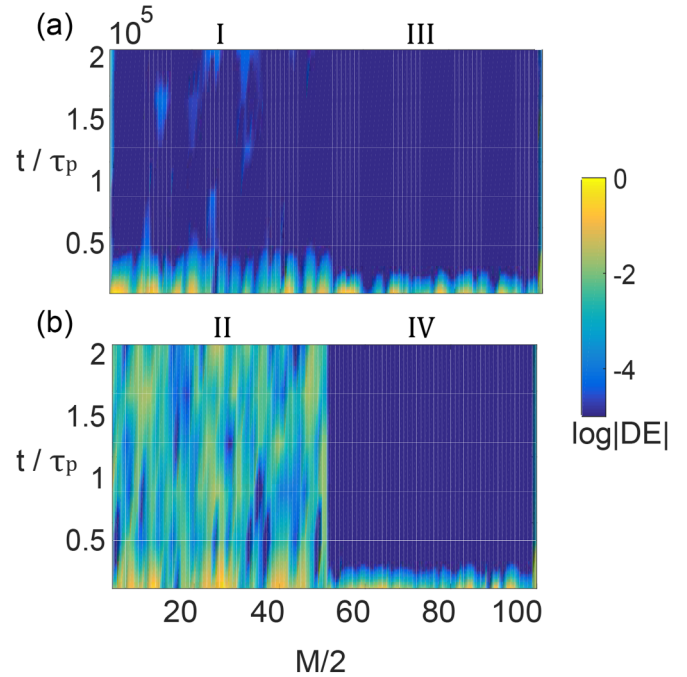
to this configuration is plotted in Fig. 12(c). The coupling strength $\eta = 0.0005$ is sufficient to induce high-amplitude oscillations for the middle laser, while the remaining part of the system is unaffected by the middle laser's oscillations. In a similar manner, high-amplitude oscillations can be induced in more than one selected distant laser within the same array.

In all previous cases of coupled-laser arrays, including small and large arrays, it is shown that the underlying mechanism of spatially localized oscillations is based on the differential pumping in the following way: Differential pumping results in the existence of strongly asymmetric phase-locked states with significantly different electric field amplitudes [20]. These states are stable up to the Hopf bifurcation point, where they give rise to stable limit cycles that are also asymmetric both in terms of the mean values of the electric field oscillations (that are close to the asymmetric phase-locked state from which they emerged) and in terms of the electric field oscillation amplitudes [18]. In all cases, it is shown that when the pumping difference is large, the lasers with the strongest pumping have almost-constant electric field values, whereas the other lasers undergo high-amplitude oscillations as shown in Figs. 1, 3, and 5. On the other hand, small pumping differences are not capable of fixing some of the electric fields at constant values and all lasers oscillate with comparable amplitudes [18]. From the above considerations, the guidelines for achieving a specific pattern of localized amplitude oscillations are (a) to operate the
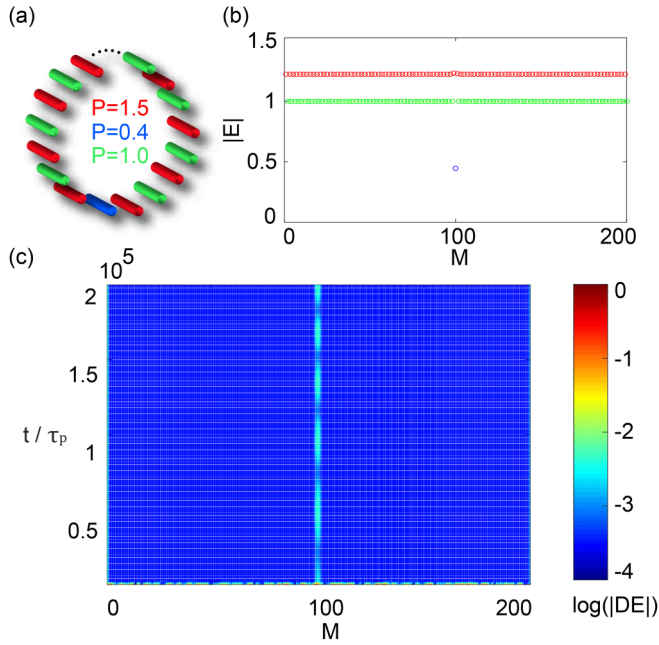
FIG. 12. (a) Schematic of a circular array where the blue laser in the middle has $P = 0.4$, while the red ones have $P = 1.5$ and the green ones $P = 1.0$. (b) Snapshots of the amplitude of the electric field in an array of $M = 200$ lasers with inhomogeneous pumping as in (a). (c) Temporal evolution of the local curvature $|DE(t)|$ on a logarithmic scale, for the whole system. The coupling strength $\eta = 0.0005$ is sufficient for large oscillations of the dimer in the middle, whereas the remaining part of the system exhibits oscillations of negligible amplitude. Other parameters: $a = 5$, $T = 400$, and $\omega_j = 0$.

system beyond the Hopf bifurcation point in order to support stable limit cycles and (b) to have significant differences in pumping strengths between the lasers with almost-fixed electric field amplitudes and the oscillating lasers, with the former having the higher pumping strengths. The appropriate pumping scheme depends weakly on the coupling strength and on the system size and the behavior of the system, whereas the output of the system is shown to be robust under the presence of random frequency detunings between the lasers.

IV. CONCLUSIONS

In conclusion, we have theoretically shown that high-amplitude oscillations coexist with very low-amplitude oscillations in small as well as large arrays of coupled lasers, depending on the distribution of their pumping rates. We have demonstrated that, by judiciously choosing the pumping rate scheme, we can control the spatial extent of the part of the array where high-amplitude oscillations take place as well as the distribution of the oscillation amplitudes within this part. Our findings provide guidelines for the generation of a desired spatially localized oscillation pattern for the output electric field, suggesting that the system has to operate beyond the Hopf bifurcation point in order to support stable self-sustained oscillations and that the pumping scheme should consist of high values of pumping rates for the lasers with constant electric field amplitudes and significantly lower values for the lasers with electric fields undergoing high-amplitude oscillations. Although the presented mechanism is capable of controlling the amplitudes, the phases of the electric fields remain, in general, uniformly distributed. The dynamical behavior of the system is also shown to be robust under different initial conditions, random frequency detuning, and different system size.

These results provide understanding of the underlying mechanism for the coexistence of high- and low-amplitude oscillations and its crucial dependence on the electrical pumping scheme. Since the latter is the most conveniently accessible parameter and can be dynamically controlled in a laser array, the results are promising for applications in reconfigurable and multifunctional photonic devices.

[1] F. Rogister and R. Roy, Phys. Rev. Lett. **98**, 104101 (2007).

[2] M. Chabanol and V. Zehnlé, Phys. Rev. A **63**, 053809 (2001).

[3] J. Shena, J. Hizanidis, N. E. Kouvaris, and G. P. Tsironis, Phys. Rev. A **98**, 053817 (2018).

[4] S. S. Wang and H. G. Winful, Appl. Phys. Lett **52**, 1774 (1988).

[5] H. G. Winful and L. Rahman, Phys. Rev. Lett. **65**, 1575 (1990).

[6] L. Fabiny, P. Colet, R. Roy, and D. Lenstra, Phys. Rev. A **47**, 4287 (1993).

[7] K. S. Thornburg, M. Möller, R. Roy, T. W. Carr, R.-D. Li, and T. Erneux, Phys. Rev. E **55**, 3865 (1997).

[8] H. G. Winful, Phys. Rev. A **46**, 6093 (1992).

[9] F. Böhm, A. Zakharova, E. Schöll, and K. Lüdge, Phys. Rev. E **92**, 069905(E) (2015).

[10] J. Shena, J. Hizanidis, V. Kovanis, and G. P. Tsironis, Sci. Rep. **7**, 42116 (2017).

[11] J. Shena, J. Hizanidis, P. Hövel, and G. P. Tsironis, Phys. Rev. E **96**, 032215 (2017).

[12] T. Erneux and P. Glorieux, *Laser Dynamics* (Cambridge University Press, Cambridge, UK, 2010).

[13] M. Parto, S. Wittek, H. Hodaei, G. Harari, M. A. Bandres, J. Ren, M. C. Rechtsman, M. Segev, D. N. Christodoulides, and M. Khajavikhan, Phys. Rev. Lett. **120**, 113901 (2018).

[14] L. Feng, R. El-Ganainy, and L. Ge, Nat. Photon. **11**, 752 (2017).

[15] L. Coldren, S. W. Corzine, and M. L. Mašanović, *Diode Lasers and Photonic Integrated Circuits* (Wiley, Upper Saddle River, NJ, 2012).

[16] Y. Kominis, V. Kovanis, and T. Bountis, Phys. Rev. A **96**, 053837 (2017).

[17] Y. Kominis, K. Choquette, V. Kovanis, and T. Bountis, Appl. Phys. Lett **113**, 081103 (2018).

[18] Y. Kominis, A. Bountis, and V. Kovanis, J. Appl. Phys. **127**, 083103 (2019).

[19] Y. Kominis, K. Choquette, V. Kovanis, and T. Bountis, IEEE Photon. J. **11**, 1500209 (2019).

[20] Y. Kominis, V. Kovanis, and A. Bountis, Phys. Rev. A **96**, 043836 (2017).

[21] A. Hohl, A. Gavrielides, T. Erneux, and V. Kovanis, Phys. Rev. Lett. **78**, 4745 (1997).

[22] M. Johnson, D. Siriani, M. Tan, and K. Choquette, Appl. Phys. Lett. **103**, 201115 (2013).

[23] S. Fryslie, M. Johnson, and K. Choquette, IEEE J. Quantum Electron. **51**, 2600206 (2015).

[24] Z. Chen, J. Liu, S. Fu, Y. Li, and B. Malomed, Opt. Express **22**, 29679 (2014).

[25] Y. Kominis, J. Cuevas-Maraver, P. Kevrekidis, D. Frantzeskakis, and A. Bountis, Chaos Solitons Fractals **118**, 222 (2019).

[26] V. Zehnlé, Phys. Rev. A **62**, 033814 (2000).

[27] H. G. Winful and S. S. Wang, Appl. Phys. Lett **53**, 1894 (1988).

[28] P. M. Varangis, A. Gavrielides, T. Erneux, V. Kovanis, and L. F. Lester, Phys. Rev. Lett. **78**, 2353 (1997).

[29] Y. Kuramoto, *Chemical Oscillations, Waves, and Turbulence* (Springer, Berlin, 1984).

[30] F. P. Kemeth, S. W. Haugland, L. Schmidt, I. G. Kevrekidis, and K. Krischer, Chaos **26**, 094815 (2016).

[31] M. J. Adams, N. Li, B. R. Cemlyn, H. Susanto, and I. D. Henning, Phys. Rev. A **95**, 053869 (2017).

[32] Z. Gao, S. T. M. Fryslie, B. J. Thompson, P. S. Carney, and K. D. Choquette, Optica **4**, 323 (2017).

[33] R. S. MacKay and S. Aubry, Nonlinearity **7**, 1623 (1994).

[34] D. Chen, S. Aubry, and G. P. Tsironis, Phys. Rev. Lett. **77**, 4776 (1996).